

Self-referenced subcycle metrology of quantum fields

Sinan Gundogdu,^{1,*} Stéphane Virally,² Marco Scaglia,² Denis V. Seletskiy,^{2,†} and Andrey S. Moskalenko^{3,‡}

¹Center for Theoretical Physics of Complex Systems,
Institute for Basic Science (IBS), Daejeon 34126, Republic of Korea

²femtoQ Lab, Department of Engineering Physics,
Polytechnique Montréal, Montréal, QC H3T 1J4, Canada

³Department of Physics, KAIST, Daejeon 34141, Republic of Korea

We propose and analyze a new time-domain method for measurement of quantum electric fields using a combination of a 3rd order nonlinear optical process and homodyne detection. Utilizing a frequency comb, this scheme yields shot-by-shot readout of quantum statistics referenced to the background noise of the classical probe. Finally, centro-symmetric character of optical nonlinearity promises novel on-chip metrology of quantum mid-infrared and terahertz fields using integrated quantum photonics.

INTRODUCTION

Homodyne detection (HD) [1] is at the heart of signal analysis in quantum optics. Briefly, a quantum state under study is interfered on a photo-diode with a strong classical mode E_{LO} , termed local oscillator (LO) [2]. HD is a frequency-domain technique, requiring spectral overlap between the two fields. Fitting for the visible and near-infrared frequency bands, HD of quantum signals in the range from mid-infrared (MIR) to terahertz (THz) is generally challenged by unavailability of strong sources of classical LO and high-efficiency photodetectors. Interest in this range is largely motivated by direct sensing opportunities afforded through commonly-strong and signature absorption features in solid-state, liquid and gaseous targets [3]. Fortunately, parallel developments in ultrafast science [4] and pulse-gated metrology [5–7] have over the years established protocols for measurement of classical fields at frequencies from THz to MIR and above [8–13]. Among these, electro-optic sampling (EOS) stands out as a particularly sensitive and experimentally accessible [5–7]. Consider a signal E_T at a low frequency Ω that co-propagates inside of a second-order ($\chi^{(2)}$) nonlinear crystal with a probe pulse E_P of bandwidth $\Delta\omega$ centered at a high frequency ω_0 (e.g. near-infrared). A second-order nonlinear mixing product ($E_T E_P$) can span over frequency $\omega_0 \pm \Omega$, in spectral overlap with the probe pulse when $2\Omega < \Delta\omega$. Mirroring the situation of HD, such spectral indistinguishability results in an interference that is exploited for the EOS detection of instantaneous amplitude E_T , resolved in time at the variable position of the probe. In contrast to HD, EOS is an intrinsically time-domain technique. Recent demonstrations ported EOS to the quantum domain, showing direct sampling of a quantum vacuum field [14, 15], and even measuring the spatio-temporal correlations [16] and causal structure of the electromagnetic ground state [17]. Such developments promise direct route toward MIR and THz quantum sensing technologies while the time-domain character moti-

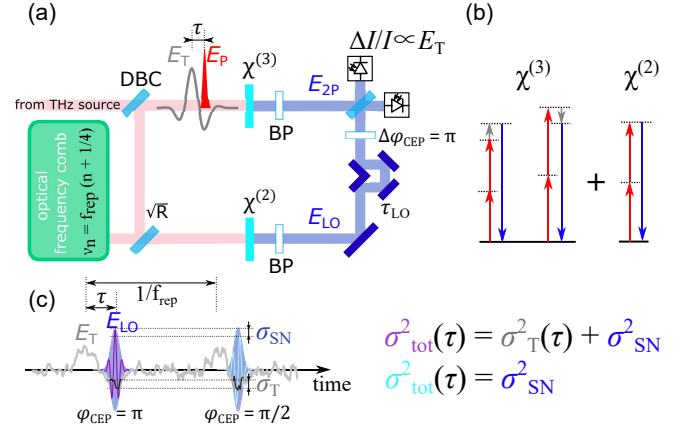


FIG. 1. (a) Proposed metrology scheme. Output of an optical comb is split in two arms. Upper arm: E_T (low-frequency signal, e.g. THz quantum vacuum) and a part of E_P (high-frequency probe pulse), time-delayed by τ , mix in a $\chi^{(3)}$ crystal to generate E_{2P} signal. Lower arm: frequency-doubled remainder of E_P in a $\chi^{(2)}$ crystal produces the pulsed local oscillator field (LO) E_{LO} . After bandpass filters (BP), E_{2P} and E_{LO} are mixed in a balanced homodyne detector. (b) Arrow diagrams highlight possible degeneracy in $\chi^{(3)}$ and $\chi^{(2)}$ outputs (red, blue and gray for E_P , E_{2P} and E_T , respectively). (c) Comb parameter $f_{CEO} = f_{rep}/4$ ensures a flip of $\Delta\phi_{CEP} = \pi/2$ between consecutive E_{LO} pulses, giving access to the variance of the quantum field $\sigma_T(\tau)$ and the shot-noise-limited background given by σ_{SN} .

vates new metrology protocols [18–20] as well as a path toward experimental quantum electrodynamics in space-time [17, 21–24]. Despite this, EOS suffers from one intrinsic drawback: there exists no simple protocol for referencing the variance of the total signal (containing the quantum contribution), to that of the background, given by the shot-noise floor of the E_P [15].

In this Letter we propose a new metrology scheme for time-domain analysis of quantum signals based on the third-order nonlinear interaction between quantum E_T and classical E_P . It opens new opportunities supplementing those available with the EOS technique. First,

utilization of centro-symmetric $\chi^{(3)}$ susceptibility significantly expands the portfolio of suitable nonlinear media, in particular promising time-domain metrology of MIR and THz quantum fields directly on integrated quantum photonics [25, 26] platforms. The need for higher input fields to engage four-wave mixing processes is elegantly addressed by the tight mode cross-sections and long interaction lengths in dispersion-managed MIR-compatible waveguides, such as e.g. Ge-on-Si [27]. Second, and in contrast to the EOS, the new scheme admits full access to the interference term via an auxiliary E_{LO} . More specifically, nonlinear mixing product $E_P E_P E_T$ at frequencies $2\omega_0 \pm \Omega$ can now be superposed with a user-controlled E_{LO} at $2\omega_0$. We show this opens an elegant opportunity for direct self-referenced measurement of the noise background via implementation of a frequency comb with a controlled carrier-envelope offset-frequency. Finally, the new scheme does not require analysis of the polarization state of the probe, relaxing constraints on broadband polarization optics [19] and promising high-sensitivity imaging modality of THz and MIR fields.

GENERATION OF THE TFISH AND LO FIELDS

Figure 1 shows the schematic of the new metrology scheme. It consists of two paths. The upper path combines E_T , the THz signal to be characterized, and the reflected part of the NIR probe pulse $E'_P = \sqrt{R}E_P$, with a central frequency ω_0 , passing through a $\chi^{(3)}$ nonlinear crystal to generate the TFISH signal E_{2P} . In the lower path the transmitted part of the probe $\sqrt{1-R}E_P$ undergoes a broadband second harmonic generation (SHG) process in a $\chi^{(2)}$ nonlinear crystal, to generate the LO pulse E_{LO} centered at $2\omega_0$ in the frequency domain. Then E_{2P} is mixed with E_{LO} at the beamsplitter to be analysed by the balanced homodyne detection technique. Unnecessary frequency content is blocked in both paths by bandpass filters that only transmit light in the frequency range around $2\omega_0$. There is a possibility to tune the time delay τ_2 between E_{2P} and E_{LO} by a variable delay line in the lower path. Independently, the phase of the LO field can be controlled by a broadband phase shifter. A shutter element resembles the option to block both the incoming probe and the THz field. In such a case in the following part of the setup the LO field is homodyned just with the quantum vacuum at the LO frequencies, providing us with a reference signal corresponding to the background vacuum of the LO. In other words it gives then just the shot noise of the LO.

The total electric field passing through the $\chi^{(3)}$ crystal, E , can be then represented as a sum: $E = E'_P + E_{2P} + E_T$. In the case when E_T corresponds to an essentially quantum field, we should describe it as well as E_{2P} and E as operators, denoting them then further as \hat{E}_T , \hat{E}_{2P} and \hat{E} . Since the probe is a strong coherent field it is

sufficient here to describe it classically using the corresponding mean value $\langle \hat{E}'_P \rangle \equiv E'_P$.

In order to describe the generation of \hat{E}_{2P} we consider the following form of the third order induced nonlinear polarization:

$$\hat{P}_{2P}^{NL} = 3\epsilon_0\chi^{(3)}RE'_P E'_P [\hat{E}_T^{(+)} + \hat{E}_T^{(-)}] + \text{H.c.}, \quad (1)$$

where we have decomposed E'_P (\hat{E}_T) into its positive $E'_P^{(+)}$ ($\hat{E}_T^{(+)}$) and negative $E'_P^{(-)}$ ($\hat{E}_T^{(-)}$) frequency parts [28]. ϵ_0 is the vacuum permittivity. We have assumed that the interaction can be well described by an effective $\chi^{(3)}$ constant, neglecting its frequency dependence. Further, we consider such a crystal orientation that it is sufficient to include only one linear polarization component for each of the involved fields. We ignore any other third order nonlinear polarization terms since they are comparably much weaker, due to the fact that E'_P is a strong coherent field and \hat{E}_T is a weak quantum signal, or the corresponding generated field contributions are removed by the bandpass filter before the beamsplitter BS₂ of the homodyning part. Under these assumptions, we can describe the electromagnetic wave propagation in the $\chi^{(3)}$ crystal using the inhomogeneous wave equation within the slowly varying amplitude approximation (SVAA) for plane waves. We decompose all fields, $X = E'_P, \hat{E}_T, \hat{E}_{2P}, \hat{P}_{NL}$, into forward-propagating plane waves as $X(z, t) = \int_0^\infty X(z, \omega) e^{i[k(\omega)z - \omega t]} d\omega + \text{H.c.}$ using a convention $X(z, \omega) \equiv 0$ for $\omega < 0$, $X^{(+)}(z, \omega) \equiv X(z, \omega)$, and $X^{(-)}(z, -\omega) = [X(z, \omega)^{(+)}]^\dagger$, which has to be taken into account for convolutions we define below. Then solving the propagation equation for the TFISH under the assumptions of small crystal thickness d and negligible depletion of the probe, we obtain (cf. Supplement 1):

$$\hat{E}_{2P}(\omega_2) = idA_P^2 C(\omega_2) (\mathcal{R} * (\hat{E}_T^{(+)} + \hat{E}_T^{(-)}))(\omega_2) + \hat{E}_B(\omega_2). \quad (2)$$

Here $*$ denotes convolution and $C(\omega) = 3\chi^{(3)}R\omega/[2cn(\omega)]$, where $n(\omega)$ is the frequency-dependent refractive index and c is the speed of light in vacuum. We decomposed $E_P = A_P f(\omega)$ into its (real) amplitude A_P and (generally complex) normalized frequency distribution $f(\omega)$, defining a gating function $\mathcal{R}(\omega_2) = (f * f)(\omega_2) e^{-i\omega_2\tau}$. The time τ corresponds to the center of the probe pulse and thus determines at which moment the incoming THz field is sampled. Finally, we introduced $\hat{E}_B(\omega_2)$, the co-propagating background vacuum field, existing in the absence of the probe field. Thus this vacuum field can be directly characterized in the current setup for a reference by switching off the probe at the upper path, as mentioned above. Here, the characterization of the background-vacuum reference signal is straightforward comparing with the original $\chi^{(2)}$ -based setup, where technically involved stretching of the probe was required [14]. In

the above derivation, we have neglected the back-action effect of the $\chi^{(3)}$ interaction on the co-propagating THz field \hat{E}_T . That is appropriate if the first term on the right-hand side of (2) represents a small correction to the second term.

TIME-RESOLVED HOMODYNE DETECTION

For the homodyne detection, we let \hat{E}_{2P} interfere with the LO field E_{LO} which is produced via the SHG in the $\chi^{(2)}$ crystal. The SHG process can be realized so that it has a high conversion efficiency η_2 and the resulting mode $f_{LO}(\omega)$ of the LO still closely resembles the mode of the TFISH field. For the details of a possible realization see Supplement 1. Since the LO represents a strong coherent field, we can describe it classically for the homodyning part of the setup. At the beam-splitter BS_2 before the detectors we can write it in the frequency domain as $E_{LO}(\omega_2) = Ae^{-i\phi}e^{-i\omega_2\tau}f_{LO}(\omega_2)$, where $A = \sqrt{\eta_2}\sqrt{1-RA_P}$ is the amplitude and ϕ is a variable phase induced by the phase shifter PS. We assume the LO has effectively the same time delay τ as the TFISH field because of the equal optical path lengths corresponding to the upper and lower arms of the setup. To assure that this is completely fulfilled in experiment, an additional tuning by τ_2 is available (Fig. 1).

The operator for the signal we are interested in is given by the difference of number of photons between the photodetectors PD_1 and PD_2 , $\hat{N}_2 - \hat{N}_1 \equiv \hat{S}_{\text{hom}}$, with

$$\hat{S}_{\text{hom}} = C'A \int_0^\infty \frac{d\omega_2}{\hbar\omega_2} n(\omega_2)\eta(\omega_2)e^{i\phi} f_{LO}^*(\omega_2)\hat{E}_{2P}(\omega_2) + \text{H.c.}, \quad (3)$$

where $C' = 4\pi c\epsilon_0 F$, F is the effective detection area and $\eta(\omega)$ is the frequency-dependent quantum efficiency of the photodetectors. Using the decomposition of \hat{E}_{2P} given by (2), we can write \hat{S}_{hom} as $\hat{S}_{\text{hom}} = \hat{S} + \hat{S}_B$, with \hat{S}_B corresponding to the background vacuum signal, and

$$\hat{S}(\tau) = C'' \int_0^\infty d\Omega \mathcal{G}_\phi(\Omega)e^{-i\Omega\tau}\hat{E}_T(\Omega) + \text{H.c.}, \quad (4)$$

where $C'' = 6\pi\epsilon_0 F d\chi^{(3)}\sqrt{\eta_2}R\sqrt{1-RA_P^3}/\hbar$ and the resulting gating function, limiting the effective integration range in (4) to THz frequencies, is given by

$$\begin{aligned} \mathcal{G}_\phi(\Omega) &= ie^{i\phi}\mathcal{G}_-(\Omega) - ie^{-i\phi}\mathcal{G}_+(\Omega); \\ \mathcal{G}_\pm(\Omega) &= \int_0^{\omega_{\text{cut}}} d\omega_2 \eta(\omega_2)f_{LO}^*(\omega_2)(f * f)(\omega_2 \pm \Omega). \end{aligned} \quad (5)$$

We have introduced ω_{cut} to represent a spectral limit induced by the filters. Deriving (4), we switched the order of integrations between the integral of (3) and that of the convolution coming there from (2). Casting the electric field operator in terms of creation $a_T^\dagger(\Omega)$ and annihilation $a_T(\Omega)$ operators, leading to $\hat{E}_T(\Omega) =$

$-i\sqrt{\hbar\Omega/C'n(\Omega)}\hat{a}_T(\Omega)$ for $\Omega > 0$, the TFISH induced contribution to the homodyne signal can be rearranged as

$$\hat{S}(\tau) = \frac{-iC''}{\sqrt{C'}} \int_0^\infty \frac{d\Omega\sqrt{\hbar\Omega}}{\sqrt{n(\Omega)}} \mathcal{G}_\phi(\Omega)e^{-i\Omega\tau}\hat{a}_T(\Omega) + \text{H.c.} \quad (6)$$

In order to obtain the quantum statistics of the operator $\hat{S}(\tau)$ at each time delay τ from the general equations (6) or (4) and thus to get access to the time-resolved properties of the quantum field \hat{E}_T , we need to assume a particular form of this field.

The simplest case for the consideration is provided by the bare THz vacuum field. In this case, the mean values of both contributions to \hat{S}_{hom} vanish. Further, since these contributions are determined by creation/annihilation operators stemming from different frequency ranges they are uncorrelated. Thus the total variance is given by the sum of the variance of the TFISH part,

$$\langle \hat{S}^2 \rangle_{\text{vac}} = \langle 0|\hat{S}^2|0\rangle = \frac{C''^2}{C'} \int_0^\infty \frac{d\Omega\hbar\Omega}{n(\Omega)} |\mathcal{G}_\phi(\Omega)|^2, \quad (7)$$

and of the variance originating from the background vacuum in the range of ω_2 frequencies,

$$\langle \hat{S}_B^2 \rangle = A^2 C' \int_0^\infty \frac{d\omega_2}{\hbar\omega_2} |f_{LO}(\omega_2)|^2 \eta^2(\omega_2) n(\omega_2). \quad (8)$$

Both variances are independent of the time delay τ . The TFISH part is determined by the properties of the gating function $\mathcal{G}_\phi(\Omega)$, which follow from the relation between $\mathcal{G}_+(\Omega)$ and $\mathcal{G}_-(\Omega)$ and can be influenced by the phase shift ϕ . When the temporal profiles of the TFISH and SHG signals coincide, we have $\mathcal{G}_+(\Omega) = \mathcal{G}_-(\Omega)$. Then $\mathcal{G}_\phi(\Omega)$ is real and vanishes for $\phi = 0$. Its absolute value is maximized for $\phi = \pm\pi/2$, with $|\mathcal{G}_\phi(\Omega)| = |\mathcal{G}_+(\Omega) + \mathcal{G}_-(\Omega)| = 2|\text{Re}(\mathcal{G}_+(\Omega))|$, representing the optimal configuration for the sampling of the THz vacuum.

In order to sample THz quantum fields beyond the bare vacuum we need to get access to both generalized quadratures of the sampled field in the time domain [18, 19, 22]. This is possible to achieve with a variation of the proposed setup, introducing an asymmetry between $\mathcal{G}_+(\Omega)$ and $\mathcal{G}_-(\Omega)$ contributions to $\mathcal{G}_\phi(\Omega)$. One of the easiest ways to realize this, suitable for our discussion here is based on the cuts in the spectra of the detected photons that can be implemented via the corresponding frequency bandpass filters [19, 24]. Looking at the second line of (5) one can anticipate that, e.g., for a bandpass filter cutting the frequencies above the central frequency of the LO, $\mathcal{G}_-(\Omega)$ dominates over $\mathcal{G}_+(\Omega)$ in terms of the absolute magnitude and $\mathcal{G}_\phi(\Omega)$ becomes complex. In the easiest case, it can be written as $\mathcal{G}_\phi(\Omega) = |\mathcal{G}_\phi(\Omega)|e^{i\theta}$, where the phase $\theta = \theta(\phi)$ is uniquely determined by the phase ϕ (and vice versa) whereas being independent of frequency.

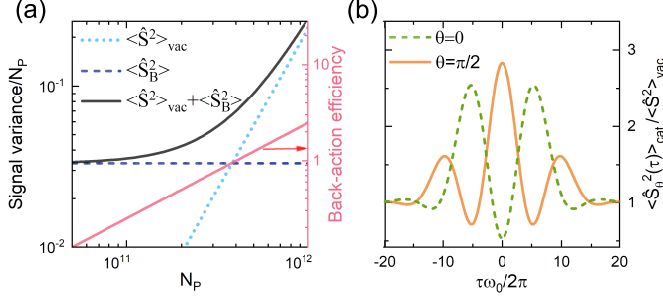


FIG. 2. (a) Normalized (by the mean probe photon number N_P) signal variance arising from the THz vacuum $\langle \hat{S}^2 \rangle_{\text{vac}}$ and the background LO vacuum $\langle \hat{S}_B^2 \rangle$ as well as the corresponding (normalized) total variance are shown as functions of N_P , along with a perturbative estimation for the back-action efficiency of the $\chi^{(3)}$ process. Parameter values: $\eta=1$, $\eta_2=0.1$, $R=2/3$, $d = 12 \mu\text{m}$, $\sigma/(2\pi) = 31 \text{ THz}$, $\omega_0/(2\pi) = 193 \text{ THz}$, $\chi^{(3)} = 2.5 \times 10^{-21} \text{ m}^2/\text{V}^2$, $n=2.4$, $F = 9 \mu\text{m}^2$. (b) TFISH signal variance for a broadband cat state, normalized by its bare vacuum counterpart. Both generalized quadratures, corresponding to $\theta = 0$ and $\theta = \pi/2$, respectively, are shown in dependence on the time delay τ . The cat state is composed of two broadband coherent states, with opposite amplitudes having Gaussian frequency distributions of central frequency $\Omega_{\text{THz}} = 0.26\omega_0$ and width $\sigma_{\text{THz}} = 0.13\omega_0$, so that the mean photon number is $\langle \text{cat} | \hat{N} | \text{cat} \rangle = 1$. For detection, $\omega_{\text{cut}} = 2\omega_0$ is used.

In particular, we have $\theta = \pi/2$ for $\phi = 0$ and $\theta = 0$ for $\phi = -\pi/2$. Then we can introduce operators $\hat{S}_0(\tau)$ and $\hat{S}_{\pi/2}(\tau)$, with $\phi = -\pi/2$ and $\phi = 0$ in (4), respectively. These operators determine both generalized quadratures of the sampled quantum field, up to frequency-dependent normalization prefactors.

RESULTS

Let us first illustrate how the proposed scheme for sampling of quantum fields operates in the case when we apply it to the bare THz vacuum, using typical experimental parameters. We assume that the probe is Gaussian, has central frequency ω_0 and spectral width σ . The LO field has central frequency $2\omega_0$ and spectral width $\sqrt{2}\sigma$. Ignoring dispersion and assuming a flat response for the detector, i.e., $n(\omega_2) = n$ and $\eta(\omega_2) = \eta$ as well as no spectral cuts for the detected photons, meaning $\omega_{\text{cut}} = \infty$ in (5), gives $\mathcal{G}_{\pm}(\Omega) = \eta \exp(-\Omega^2/8\sigma^2)/2\sqrt{2\pi}\sigma$. The TFISH contribution to the variance is maximized for $\phi = -\pi/2$, with $\mathcal{G}_{\phi}(\Omega) = 2\mathcal{G}_{+}(\Omega)$ here. We get then

$$\langle \hat{S}^2 \rangle_{\text{vac}} = \frac{9d^2\eta^2\eta_2(1-R)R^2\sigma^3(\chi^{(3)})^2\omega_0^3\hbar^2}{8\pi^{3/2}c^4n^4\epsilon_0^2F^2} N_P^3, \quad (9)$$

where $N_P = A_P^2 n C' \int_0^\infty \frac{f^2(\omega) d\omega}{\hbar\omega} \approx \frac{A_P^2 n C'}{2\sqrt{\pi}\hbar\sigma\omega_0}$ is the average number of photons in the probe. Under the same

conditions we obtain

$$\langle \hat{S}_B^2 \rangle \approx A^2 C' \frac{n\eta^2}{2\sqrt{\pi}\hbar\sigma\omega_0} = \eta^2\eta_2(1-R)N_P. \quad (10)$$

Figure 2 shows $\langle \hat{S}^2 \rangle_{\text{vac}}$, $\langle \hat{S}_B^2 \rangle$ and the total variance $\langle \hat{S}_{\text{hom}}^2 \rangle$ as functions of the number of photons in the probe pulse, contrasted with an estimation of the back-action efficiency of the $\chi^{(3)}$ process in the perturbative regime (see Supplement 1 for details). We choose the parameters considering a probe laser with $1.55 \mu\text{m}$ central wavelength and 6 fs pulse duration and a thin $12 \mu\text{m}$ slab of diamond for the $\chi^{(3)}$ crystal. The variance of the TFISH part surpasses the variance due to the background vacuum at around $N_P = 3.7 \times 10^{11}$ photons per pulse. However, the back-action becomes significant around the same photon number, invalidating then the utilized perturbative approach. To prevent this, N_P can be chosen at a lower value, implementing a weak measurement. To achieve the required signal to noise ratio, the measurement results can be then averaged over a sufficient number of probe pulses, as in [14, 16, 21].

As an illustration of the scheme going beyond sampling of the THz quantum vacuum, Fig. 2(b) shows the variance signals for a broadband cat state, as a function of the time delay of the probe. The utilized cat state is defined as $|\text{cat}\rangle \propto |\{\alpha_\Omega\}\rangle + |{-\alpha_\Omega}\rangle$, where $|\{\alpha_\Omega\}\rangle$ represents a continuous multimode coherent state with the spectral amplitudes α_Ω corresponding to a classical few-cycle THz pulse [29, p. 85]. To access both quadratures, we performed the frequency cut on the spectral content of the photons collected by the photodetectors, determining the gating function (5), by choosing $\omega_{\text{cut}} = 2\omega_0$. Further details on the calculation are given in Supplement 1.

CONCLUSION

We have developed a new scheme for sampling of quantum fields in the time domain and illustrated it by calculating the electric-field variance and its dynamics for the quantum vacuum and a pulsed broadband cat state, respectively. The scheme is feasible for typical experimental parameters and offers significant advantages over the recently established quantum electro-optic sampling. In particular, it enables subtracting of the contaminating shot-noise by the shot-by-shot self-referencing, without changing any geometrical parameters. The independent tunability of the local oscillator strength in the $\chi^{(2)}$ part of the setup offers additional freedom in control of the experimental sensitivity in terms of the signal-to-noise ratio. Employing additional frequency filters in the homodyning part, it is possible to sample both generalized electric-field quadratures, opening the door to the realization of the subcycle quantum tomography.

National Research Foundation of Korea (NRF) grant funded by the Korea government

(MSIT)(2020R1A2C1008500); Mercator Fellowship of the Deutsche Forschungsgemeinschaft (DFG) - Project No. 425217212 - SFB 1432; Baden-Württemberg Stiftung via the Elite Programme for Postdocs; Institute for Basic Science in Korea (IBS-R024-D1).

* gu.sinan@gmail.com

† denis.seletskiy@polymtl.ca

‡ moskalenko@kaist.ac.kr

- [1] M. Collett, R. Loudon, and C. Gardiner, *Journal of Modern Optics* **34**, 881 (1987).
- [2] A. I. Lvovsky and M. G. Raymer, *Rev. Mod. Phys.* **81**, 299 (2009).
- [3] A. Schliesser, N. Picqué, and T. Hänsch, *Nature Photonics* **6**, 440 (2012).
- [4] F. Krausz and M. Ivanov, *Rev. Mod. Phys.* **81**, 163 (2009).
- [5] Q. Wu and X. Zhang, *Applied Physics Letters* **67**, 3523 (1995).
- [6] G. Gallot and D. Grischkowsky, *Journal of the Optical Society of America B* **16**, 1204 (1999).
- [7] A. Leitenstorfer, S. Hunsche, J. Shah, M. C. Nuss, and W. H. Knox, *Applied Physics Letters* **74**, 1516 (1999).
- [8] Q. Wu and X.-C. Zhang, *Applied Physics Letters* **71**, 1285 (1997).
- [9] C. Kübler, R. Huber, S. Tübel, and A. Leitenstorfer, *Applied Physics Letters* **85**, 3360 (2004).
- [10] P. Gaal, M. B. Raschke, K. Reimann, and M. Woerner, *Nature Photonics* **1**, 577 (2007).
- [11] A. Sell, R. Scheu, A. Leitenstorfer, and R. Huber, *Applied Physics Letters* **93**, 251107 (2008).
- [12] S. Keiber, S. Sederberg, A. Schwarz, M. Trubetskov, V. Pervak, F. Krausz, and N. Karpowicz, *Nature Photonics* **10**, 159 (2016).
- [13] C. Riek, D. V. Seletskiy, and A. Leitenstorfer, *Eur. J. Phys.* **38**, 024003 (2017).
- [14] C. Riek, D. V. Seletskiy, A. S. Moskalenko, J. F. Schmidt, P. Krauspe, S. Eckart, S. Eggert, G. Burkard, and A. Leitenstorfer, *Science* **350**, 420 (2015).
- [15] A. S. Moskalenko, C. Riek, D. V. Seletskiy, G. Burkard, and A. Leitenstorfer, *Phys. Rev. Lett.* **115**, 263601 (2015).
- [16] I.-C. Benea-Chelmus, F. F. Settembrini, G. Scalari, and J. Faist, *Nature* **568**, 202 (2019).
- [17] F. F. Settembrini, F. Lindel, A. M. Herter, S. Y. Buhman, and J. Faist, “Detection of quantum-vacuum field correlations outside the light cone,” (2021), arXiv:2111.02377 [quant-ph].
- [18] S. Virally and B. Reulet, *Phys. Rev. A* **100**, 023833 (2019).
- [19] P. Sulzer, K. Oguchi, J. Huster, M. Kizmann, T. L. M. Guedes, A. Liehl, C. Beckh, A. S. Moskalenko, G. Burkard, D. V. Seletskiy, and A. Leitenstorfer, *Phys. Rev. A* **101**, 033821 (2020).
- [20] S. Virally, P. Cusson, and D. V. Seletskiy, *Phys. Rev. Lett.* **127**, 270504 (2021).
- [21] C. Riek, P. Sulzer, M. Seeger, A. S. Moskalenko, G. Burkard, D. V. Seletskiy, and A. Leitenstorfer, *Nature* **541**, 376 (2017).
- [22] M. Kizmann, T. L. M. Guedes, D. V. Seletskiy, A. S. Moskalenko, A. Leitenstorfer, and G. Burkard, *Nat. Phys.* **15**, 960 (2019).
- [23] F. Lindel, R. Bennett, and S. Y. Buhmann, *Phys. Rev. A* **102**, 041701 (2020).
- [24] M. Kizmann, A. S. Moskalenko, A. Leitenstorfer, G. Burkard, and S. Mukamel, “Quantum susceptibilities in time-domain sampling of electric field fluctuations,” arXiv:2103.07715.
- [25] K.-H. Luo, S. Brauner, C. Eigner, P. R. Sharapova, R. Ricken, T. Meier, H. Herrmann, and C. Silberhorn, *Science Advances* **5**, eaat1451 (2019).
- [26] I.-C. Benea-Chelmus, Y. Salamin, F. F. Settembrini, Y. Fedoryshyn, W. Heni, D. L. Elder, L. R. Dalton, J. Leuthold, and J. Faist, *Optica* **7**, 498 (2020).
- [27] U. Griskeviciute, R. W. Millar, K. Gallacher, J. Valente, and D. J. Paul, *Opt. Express* **28**, 5749 (2020).
- [28] R. J. Glauber, *Phys. Rev.* **130**, 2529 (1963).
- [29] W. Vogel and D. Welsch, *Quantum Optics*, 3rd ed. (Wiley, Weinheim, 2006).